Published in final edited form as:
J Mater Sci Mater Med. 2011 June ; 22(6): 1465–1477. doi:10.1007/s10856-011-4325-4.

Characterization of and host response to tyramine substituted-hyaluronan enriched fascia extracellular matrix

LiKang Chin,
Department of Biomedical Engineering, Lerner Research Institute, Cleveland Clinic, 9500 Euclid Avenue, ND20, Cleveland, OH 44195, USA. Department of Biomedical Engineering, Case Western Reserve University, Cleveland, OH 44106, USA

Anthony Calabro,
Department of Biomedical Engineering, Lerner Research Institute, Cleveland Clinic, 9500 Euclid Avenue, ND20, Cleveland, OH 44195, USA

E. Rene Rodriguez,
Department of Anatomic Pathology, Cleveland Clinic, Cleveland, OH 44195, USA

Carmela D. Tan,
Department of Anatomic Pathology, Cleveland Clinic, Cleveland, OH 44195, USA

Esteban Walker, and
Department of Quantitative Health Sciences, Cleveland Clinic, Cleveland, OH 44195, USA

Kathleen A. Derwin
Department of Biomedical Engineering, Lerner Research Institute, Cleveland Clinic, 9500 Euclid Avenue, ND20, Cleveland, OH 44195, USA

Kathleen A. Derwin: derwink@ccf.org

Abstract

Naturally-occurring biomaterial scaffolds derived from extracellular matrix (ECM) have been previously investigated for soft tissue repair. We propose to enrich fascia ECM with high molecular weight tyramine substituted-hyaluronan (TS-HA) to modulate inflammation associated with implantation and enhance fibroblast infiltration. As critical determinants of constructive remodeling, the host inflammatory response and macrophage polarization to TS-HA enriched fascia were characterized in a rat abdominal wall model. TS-HA treated fascia with cross-linking had a similar lymphocyte ($P = 0.11$) and plasma cell ($P = 0.13$) densities, greater macrophage ($P = 0.001$) and giant cell ($P < 0.0001$) densities, and a lower density of fibroblast-like cells ($P < 0.0001$) than water treated controls. Treated fascia, with or without cross-linking, exhibited a predominantly M2 pro-remodeling macrophage profile similar to water controls ($P = 0.82$), which is suggestive of constructive tissue remodeling. Our findings demonstrated that HA augmentation can alter the host response to an ECM, but the appropriate concentration and molecular weight needed to minimize chronic inflammation within the scaffold remains to be determined.

1 Introduction

Acellularized scaffolds derived from extracellular matrix (ECM) have been investigated for soft tissue repair and reconstruction in both animal and human clinical studies for a variety

Correspondence to: Kathleen A. Derwin, derwink@ccf.org.

of applications in the cardiovascular [1–3], gastrointestinal [4, 5], urological [6, 7], dermatological [8, 9], and orthopaedic fields [9–11]. These naturally-occurring biomaterials are particularly attractive due to their native three-dimensional architecture that is a composite of structural and functional proteins [12, 13]. Macromolecules native to the ECM are believed to modulate host processes such as cell migration and proliferation, angiogenesis, and the inflammatory response, potentially in a manner that will enhance and accelerate the biology of tissue repair [12, 13]. The use of acellular ECM scaffolds that are subsequently populated by host cells eliminates the challenges of cell harvesting, viability, and immunocompatibility associated with cell-delivery tissue engineering approaches [14, 15]. The ideal scaffold material would serve as an inductive template with the appropriate mechanical properties to prevent or limit tissue re-tear during the course of remodeling and would facilitate downstream integration/reconstruction of functional tissue [12, 16]. Our laboratory has focused on scaffolds derived from human fascia lata ECM because fascia has robust material properties with an average elastic modulus of ~530 MPa [17, 18].

The host inflammatory response, including the macrophage component, appears to be a critical determinant, and perhaps predictor, of successful and constructive remodeling of an implanted biomaterial [19, 20]. Based on microenvironmental cues from cytokines or microbial products, macrophages demonstrate their plasticity by exhibiting certain phenotypic markers, expression profiles, and cellular functions [19, 21–23]. Consequently, macrophage phenotypes span a continuous spectrum, the two extremes of which are represented by the M1 pro-inflammatory and M2 pro-remodeling activated forms [24]. M1 macrophages produce large amounts of reactive oxygen species and inflammatory cytokines, express CCR7 as a cell surface marker, and are associated with tissue destruction and inflammation [19, 24]. Macrophages of the M2 phenotype are characterized by CD163 as a cell surface marker and are associated with angiogenesis as well as tissue repair and remodeling [19, 24].

We propose to enrich fascia ECM with exogenous high molecular weight hyaluronan (HA) to improve fascia's ability to facilitate soft tissue repair by modulating inflammation and enhancing fibroblast infiltration. Well-known for its roles in morphogenesis, wound repair, and inflammation, HA has a myriad of properties that are highly dependent on molecular weight [25–27]. High molecular weight HA is most often recognized for its anti-inflammatory properties, and numerous studies have demonstrated that exogenous HA can inhibit the infiltration, proliferation, and cytokine production of various inflammatory cells [28–31]. In addition, HA has been shown to promote the migration of fibroblasts [32, 33]. In contrast, low molecular weight HA elicits pro-inflammatory responses, such as increased production of nitric oxide as well as other pro-inflammatory mediators [34–36].

The current study investigates the use of high molecular weight tyramine substituted-hyaluronan (TS-HA), which has tyramine adducts coupled to the carboxyl groups of the glucuronic acid residues along 5% of the HA chain [37]. In the presence of hydrogen peroxide and peroxidase, neighboring tyramine adducts cross-link to form a dityramine bridge. The resulting hydrogel is not susceptible to hydrolysis and has a concentration-dependent resistance to hyaluronidase degradation [37]. By means of tyramine cross-linking, high molecular weight HA can be immobilized within fascia ECM, thus providing a sustained presence of HA to the repair site. However, the extent to which high molecular weight HA can modulate the host response to fascia ECM, particularly in a manner which would promote a constructive remodeling outcome, has not been previously investigated.

Thus, the objective of this work was to characterize the host inflammatory response and macrophage polarization to HA enriched fascia ECM. We first characterized the content, distribution, and retention of TS-HA, with and without cross-linking, within fascia following

a diffusion-based treatment method. We then investigated the host response to fascia enriched with 5–10 micrograms of HA per milligram of dry weight tissue (μg/mg) in a rat abdominal wall defect model. The presence of various inflammatory cells, non-inflammatory cells, total cellularity, vascularity, and macrophage polarization into the M1 and M2 phenotypes were scored. We hypothesized that TS-HA treated fascia with cross-linking would exhibit lower lymphocyte, plasma cell, macrophage, and giant cell densities, higher fibroblast-like cell density, and a greater proportion of M2 macrophages than M1 macrophages when compared to water treated controls and treated fascia without cross-linking.

2 Materials and methods

2.1 Experimental design

Decellularized, lyophilized, sterile human fascia lata derived from the iliotibial tract of donors aged 18–55 years was obtained from the Musculoskeletal Transplant Foundation (Edison, NJ). Fascia patches (5 × 5 cm) were distributed into three treatment groups: water treated controls, TS-HA with cross-linking, and TS-HA without cross-linking (n = 8–20 patches per group). After treatment, HA content was quantified. TS-HA treated fascia patches with a mean concentration of 5–10 μg/mg were selected for subsequent experiments (n = 8 per group). Each fascia patch was then divided into samples that were used for an in vitro retention experiment, HA staining, and rat abdominal wall implantation at two time points. Forty-eight rats were used for the host response study (n = 16 per treatment group). Rats were sacrificed at 1 and 3 months (n = 8 per group per time point), and the implants were harvested for histologic analysis of cell types and vascularity. Detailed methods are described below.

2.2 TS-HA treatment of fascia

For the two TS-HA treatment groups, each fascia patch (5 × 5 cm) was rehydrated in 30 ml of 0.75% TS-HA solution (0.9–1 M Da MW, Lifecore Biomedical, Chaska, MN) in ultrapure water for 24 h at 37°C on a shaker. The solutions used to treat cross-linked patches also contained 10 U/ml of horseradish peroxidase (Sigma, St. Louis, MO). After treatment, the patches were rinsed once in 30 ml of ultrapure water for 30 s and blotted two times per side on a sterile towel to remove excess surface TS-HA. Treated patches in the uncross-linked group were then rinsed in 125 ml of ultrapure water for 5–20 min at 37°C on a shaker. Patches in the cross-linked group were submerged in 30 ml of a 0.3% hydrogen peroxide solution (Fisher, Pittsburgh, PA) in ultrapure water for 30 s at room temperature with slight agitation and then allowed to sit covered on a glass dish at 4°C for the reaction to continue overnight. Cross-linked patches were subsequently rinsed with 125 ml of ultrapure water for 24 h at 37°C on a shaker to remove excess horseradish peroxidase, hydrogen peroxide, and any uncross-linked TS-HA. Fascia patches rehydrated in 30 ml of ultrapure water for 24 h at 37°C served as controls. All fascia patches were subsequently lyophilized.

2.3 HA content of treated fascia

From each 5 × 5 cm patch, triplicate pieces that together represented ~10% of total patch volume were used to estimate the mean HA content of the entire patch. HA content was quantified using fluorophore-assisted carbohydrate electrophoresis (FACE) according to previously described methods [17, 38]. Briefly, tissue samples were rehydrated, digested with proteinase K (PK, Fisher Biotech, Fair Lawn, NJ), centrifuged to remove undigested tissue residue, and the glycosaminoglycans (GAG) released into the supernatant fraction were isolated by ethanol precipitation. After extensive digestion of the resuspended ethanol pellet with hyaluronidase Streptococcus dysgalactiae (SD) and chondroitinase ABC (both from Seikagaku America, Falmouth, MA), the resulting GAG disaccharides were tagged

with the fluorophore 2-aminoacridone (AMAC, Molecular Probes, Eugene, OR), separated by electrophoresis, and the HA disaccharides were quantified using ultraviolet imaging and analysis.

All of the HA in water treated and uncross-linked TS-HA treated samples was recovered in the ethanol precipitate fraction of the PK supernatant. However, the cross-linked TS-HA treated samples required additional processing for FACE analysis, since the TS-HA hydrogel generated within the fascia by the cross-linking reaction was not solubilized by digestion with PK alone. Thus, both the PK pellet and supernatant fractions were processed for FACE analysis. The PK supernatant fraction was incubated with 18 U/ml of testicular hyaluronidase (Sigma) overnight at 37°C to solubilize cross-linked TS-HA hydrogel. A 400 μl aliquot was dried in a speed-vac and precipitated in 77% ethanol as previously described. Both the ethanol precipitate and the aspirate were dried, resuspended in 200 μl of 0.1 M ammonium acetate, pH 7.0, digested with hyaluronidase SD and chondroitinase ABC, fluorotagged with AMAC, and electrophoresed according to the standard protocol. The PK pellet fraction was resuspended in 200 μl of 1 M ammonium acetate, pH 7.0, and then precipitated in 77% ethanol, and the precipitate was subsequently digested with 5 U/ml testicular hyaluronidase for 48 h at 37°C. The hyaluronidase digest was centrifuged, and the resulting supernatant and pellet fractions were further digested with hyaluronidase SD and chondroitinase ABC, fluorotagged with AMAC, and electrophoresed according to the standard protocol. Treated fascia patches, with or without cross-linking, that had a mean TS-HA content of 5–10 μg/mg were selected for all subsequent experiments (n = 8 patches per group).

2.4 In vitro retention of HA

From each 5 × 5 cm TS-HA treated patch, with or without cross-linking, triplicate 0.8 × 1 cm pieces that together represented ~10% of the total patch volume were obtained. Each piece was rehydrated in 1.2 ml of phosphate buffered saline (PBS) and incubated for 72 h at 37°C on a shaker, after which the TS-HA content in the fascia was measured with FACE according to methods described above.

2.5 Distribution of HA in treated fascia

Representative ~0.4 × 1 cm pieces from the TS-HA with cross-linking and water control groups (n = 6 per group) were rehydrated in 100 μl of ultrapure water for 6 h at room temperature and embedded in Tissue-Tek OCT compound (Sakura Finetek, Torrance, CA). Five-micron longitudinal frozen sections were cut and fixed in a 4% paraformaldehyde/6% glacial acetic acid/82% ethanol aqueous solution [39] for 10 min, followed by three 1 min PBS rinses. Sections were blocked in 3% normal goat serum (Jackson ImmunoResearch Labs, Inc., West Grove, PA) for 30 min and incubated with biotinylated HA binding protein (bHABP, Calbiochem, San Diego, CA) diluted 1:100 in PBS in a humidified chamber at 4°C overnight. Sections were then rinsed in PBS three times for 5 min each, incubated with Alexa Fluor 488-conjugated streptavidin (Molecular Probes, Carlsbad, CA) diluted 1:500 in PBS for 45 min, and rinsed again in PBS. All steps were performed at room temperature, unless otherwise specified. Porcine cartilage served as a positive control and sections incubated with PBS in place of bHABP served as negative controls. All slides were mounted with Vectashield mounting media (Vector Labs, Burlingame, CA).

2.6 Rat abdominal wall defect model

All procedures were performed in accordance with the National Institutes of Health guidelines for care and use of laboratory animals and were approved by the Institutional Animal Care and Use Committee at the Cleveland Clinic.

Forty-eight adult, male Lewis rats were used for this study (450–600 g, Harlan, Indianapolis, IN). Each rat was anesthetized with an intramuscular injection of ketamine, xylazine, and acepromazine (30/6/1 mg/kg). The abdomen was prepared for aseptic surgery. Via a ventral midline incision, a partial-thickness 0.8 × 1 cm defect was created in the anterior sheath adjacent to the linea alba. The anterior sheath was removed and the underlying rectus muscle, transversalis fascia, and peritoneum were left intact. One 0.8 × 1 cm fascia piece from each patch was wetted in saline for 10 min, and secured into the defect using four corner sutures of 5-0 Prolene. On the contralateral side of the linea alba, a second defect (0.4 × 4.5 cm) was created and replaced with a 0.4 × 4.5 cm fascia piece, wetted as above, from the same patch for mechanical property analysis (mechanical properties data are not presented herein). The skin incision was closed using 4-0 chromic gut suture, and the rat was allowed to recover from anesthesia under a heating lamp. For analgesia, each rat received 0.15 mg/kg buprenorphine post-operatively, 12 h later, and thereafter as needed. Rats were housed individually for the duration of the study.

2.7 Euthanasia and tissue harvest

At 1 and 3 months, rats were sacrificed via carbon dioxide asphyxiation (n = 8 per group per time point). The fascia graft and underlying muscle were harvested. Half of the graft was fixed in 10% neutral buffered formalin for 24 h and routinely processed for paraffin embedding. The second half was embedded in OCT compound.

2.8 Histology and immunohistochemistry

The formalin-fixed, paraffin-embedded samples were cut into 5-μm-thick longitudinal sections and stained with hematoxylin and eosin (H&E). A subset of the OCT embedded samples (n = 4 per group per time point) were immunostained for CCR7 (a pro-inflammatory M1 macrophage maker), CD163 (a pro-remodeling M2 macrophage marker), and CD31 (an endothelial cell marker for neovascularization). Five-micron-thick, serial frozen sections were cut and fixed in acetone for 2 min. Following three 5 min PBS rinses, sections were then incubated with 1% aqueous phosphomolybdic acid to reduce fascia auto-fluorescence. Sections were rinsed again in PBS, and non-specific binding of the primary antibody was blocked using 3% normal goat serum in PBS for 2 h. After blocking, sections were incubated in primary antibody diluted with PBS in a humidified chamber at 4°C for 18 h. Sections were then incubated in biotinylated secondary antibody diluted with PBS for 1 h, then in Alexa Fluor 488-conjugated streptavidin (Molecular Probes, Carlsbad, CA) for 45 min, and finally mounted with Vectashield mounting media containing 4′,6-diamidino-2-phenylindole (DAPI) to visualize cell nuclei. After each application of antibody or streptavidin, sections were rinsed in PBS three times for 15 min. Rat spleen served as a positive control, and sections incubated with PBS in place of the primary antibody served as negative controls. The primary antibodies used in this study were: mouse anti-rat CD163 (1:600, MCA342R, AbD Serotec), rabbit anti-rat CCR7 (1:250, NB110-55678, Novus Biologicals, Littleton, CO), and mouse anti-rat CD31 (1:500, MCA1334GA, AbD Serotec). The biotinylated secondary antibodies used were: horse anti-mouse (1:100, BA-2001, Vector Labs) and goat anti-rabbit (1:200, 111-065-003, Jackson ImmunoResearch Labs).

2.9 Semi-quantitative histologic analysis

One representative H&E and immunostained section from each rat was semi-quantitatively scored by two blinded, board-certified pathologists (ERR and CDT) according to a scoring system adapted from the International Organization for Standardization (ISO) Standard 10993-6 (Table 1). H&E sections were scored for the presence of inflammatory cells—lymphocytes, plasma cells, macrophages, and giant cells. The M1 and M2 macrophage phenotypes were scored from sections immunostained for CCR7 and CD163, respectively. Non-inflammatory outcomes such as the presence of fibroblast-like cells and the amount of

cellular infiltrate into the graft from the periphery (cellularity) were scored from the H&E sections, and neovascularization was scored from CD31 immunostained sections.

2.10 Pre and post-implantation cross-sectional area

At the time of implantation, the thickness of each 0.8 × 1 cm fascia piece was aseptically measured with calipers prior to rehydration. The pre-implantation cross-sectional area of each piece was estimated as the product of the dehydrated thickness times the 1 cm height. Post-implantation cross-sectional area measurements were made by manually tracing the perimeter of the grafts from H&E stained sections using ImageScope software (Aperio Technologies, Vista, CA).

2.11 Statistical analysis

Two-way analysis of variance (ANOVA) was performed to examine the effects of treatment and time on in vitro HA content, post-implantation cross-sectional area, and all histologic outcomes. One-way ANOVA was performed to examine the effect of treatment on pre-implantation cross-sectional area. When appropriate, multiple comparisons were performed with a Tukey Honestly Significant Difference post-hoc test. In addition, to compare CD163+ M2 macrophage and CCR7+ M1 macrophage scores, a Wilcoxon signed rank test was performed. Inter-rater reliability between the two pathologists who performed the histologic scoring was evaluated by calculating kappa scores and percent agreement. For all statistical analysis, a P value of ≤0.05 was considered significant, and a P value of ≤0.10 was indicative of a trend. Results are expressed as mean ± standard deviation or mean (range).

3 Results

3.1 HA content of treated fascia

The HA content of 5 × 5 cm fascia patches used for these experiments averaged 7.6 ± 2.3 μg/mg for TS-HA treated fascia with cross-linking and 7.8 ± 1.8 μg/mg for treated fascia without cross-linking (Table 2). Thus TS-HA constituted ~1% of the tissue weight in the treated groups, which is an order of magnitude higher than the HA content in water treated controls (0.2 ± 0.1 μg/mg).

3.2 In vitro retention of TS-HA

The mean HA content of treated fascia without cross-linking decreased by ~65% following the 72 h retention experiment ($P < 0.001$), but there was no decrease from time-zero concentration for treated fascia with cross-linking (Table 2).

3.3 Distribution of HA in treated fascia

Staining of treated fascia with bHABP demonstrated that the exogenously added HA was distributed throughout the fascia matrix, primarily around large fascicle bundles (Fig. 1).

3.4 Descriptive histology

Fascia grafts of all experimental groups were still visible and discernable from the underlying muscle at 1 (Fig. 2a–c) and 3 months (Fig. 3a–c). Remnant fascia architecture was identified as acellular bundles of dense collagen, particularly within the central region of the grafts (Figs. 2d–i, 3d–i). Treated fascia with cross-linking was uniquely characterized by regions of TS-HA hydrogel which stained light blue on H&E sections and were located between collagen bundles throughout the graft (Figs. 2e, h, 3e, h). At both time points, fascia in all groups elicited a chronic inflammatory host response predominantly seen at the periphery of the grafts (Figs. 2a–c, 3a–c). The infiltrates were composed of lymphocytes, macrophages, and a variable number of plasma cells and giant cells (Figs. 2g–i, 3g–i). Of

note, there was a persistent, moderate infiltrate of giant cells at 3 months in treated fascia with cross-linking (Fig. 3h). Grafts of all groups had variable regions of dense cellularity and disorganized connective tissue, suggestive of matrix remodeling and deposition (Figs. 2d–f, 3d–f). The central region of the grafts showed variable cellularity ranging from completely acellular regions, to regions with a low density of spindle-shaped fibroblast-like cells, to tracks or pockets of dense cellular infiltrate (Figs. 2g–i, 3g–i). Treated fascia without cross-linking tended to show the highest cellularity of the three groups, in part due to infiltration of fibroblast-like cells between collagen bundles (Figs. 2i, 3i). Vascularization was observed within grafts of all groups.

3.5 Kappa scores and percent agreement

Histologic scores were assessed for agreement between the two reviewers. Kappa scores for all outcomes ranged from 0.58 to 0.89 and percent agreement was at least 71%, indicating moderate to high agreement. Since inter-rater reliability was acceptable, scores from only one reviewer (ERR) are presented in this paper.

3.6 Inflammatory cells

The mean scores for the inflammatory cell outcomes from each group at both time points are presented in Table 3. For each histologic outcome, the interaction between experimental group and time was not significant and was, therefore, dropped from the ANOVA model. There were no differences in lymphocyte or plasma cell density between groups at 1 or 3 months. Compared to water treated controls, TS-HA treated fascia with cross-linking exhibited significantly more macrophages ($P = 0.001$) and giant cells ($P < 0.0001$) at 1 and 3 months. Similarly, TS-HA treated fascia without cross-linking had significantly more macrophages than water controls ($P = 0.001$) at 1 and 3 months, but no difference in giant cells. Hence, the only difference in host response between TS-HA treatments was the significantly higher giant cell density in the cross-linked group compared to the uncross-linked group at 1 and 3 months ($P < 0.0001$). Across all groups, the density of plasma cells ($P = 0.02$) and macrophages ($P = 0.03$) in fascia grafts significantly decreased with time.

In all groups at both time points, the density of CD163+ M2 macrophages was greater than CCR7+ M1 macrophages ($P < 0.0001$), indicating that macrophage polarization was dominated by the pro-remodeling phenotype (Table 3). Neither CCR7 nor CD163 density was significantly different among experimental groups at either time point. Across all groups, the density of CD163+ M2 macrophages significantly decreased with time ($P = 0.02$). CCR7+ M1 macrophages were focally concentrated in small clusters, while CD163+ M2 macrophages were localized at the periphery of the grafts (Fig. 4).

3.7 Total cellularity

TS-HA treated fascia without cross-linking demonstrated a trend towards increased cellularity compared to water controls at 1 and 3 months (Table 4, $P = 0.09$).

3.8 Fibroblast-like cells

TS-HA treated fascia with cross-linking exhibited a significantly lower density of fibroblast-like cells than water controls ($P < 0.0001$) and treated fascia without cross-linking ($P < 0.0001$) at 1 and 3 months (Table 4). TS-HA treated fascia without cross-linking had a similar density of fibroblast-like cells as water controls at both time points.

3.9 Vascularity

CD31 scores were not significantly different among experimental groups, but there was a trend towards a decrease with time across all groups (Table 4, $P = 0.10$). CD31 staining for neovascularization was predominantly localized at the graft periphery (Fig. 5).

3.10 Pre- and post-implantation cross-sectional area

TS-HA treated fascia pieces, with ($P = 0.06$) or without cross-linking ($P = 0.08$), trended towards greater pre-implantation cross-sectional area than water controls (Fig. 6). Post-implantation cross-sectional area significantly decreased from 1 to 3 months for all groups ($P = 0.02$). There was no significant difference in cross-sectional area among groups at either post-implantation time point.

4 Discussion

In this study, we demonstrated a method of TS-HA treatment that increased the amount of HA in fascia by an order of magnitude to approximately 1% tissue weight. Furthermore, the incorporated HA was distributed throughout the tissue and, upon cross-linking, the TS-HA was retained as a hydrogel network. The effectiveness of tyramine cross-linking in immobilizing HA within fascia was validated through an in vitro retention experiment. Moreover, this study characterized the host response to TS-HA treated fascia in a rat abdominal wall defect model with the hypothesis that treated fascia with cross-linking would exhibit lower lymphocyte, plasma cell, macrophage and giant cell densities, a higher fibroblast density, and a greater proportion of M2 macrophages than M1 macrophages compared to water treated controls and treated fascia without cross-linking. In contrast, our results showed that TS-HA treated fascia with cross-linking had a similar lymphocyte and plasma cell densities, greater macrophage and giant cell densities, and a lower density of fibroblast-like cells than water treated controls. However, treated fascia with cross-linking did exhibit a predominantly M2 pro-remodeling macrophage profile, similar to water controls and treated fascia without cross-linking.

The water treated controls in this study demonstrate the host response to unmodified, decellularized fascia ECM in a xenogenic implantation model. At 3 months, water treated fascia supported a heavy population of fibroblast-like cells and a moderate degree of vascularity. A moderate macrophage infiltrate was largely of the pro-remodeling M2 phenotype. Since macrophages are key mediators of both inflammatory and anti-inflammatory pathways, classification into M1 pro-inflammatory or M2 pro-remodeling phenotypes may serve as a predictive tool for downstream outcomes following graft implantation [19, 20]. The presence of pro-remodeling macrophages and fibroblast-like cells is suggestive of host repair and tissue remodeling.

All fascia grafts were also characterized by a heavy, chronic lymphocyte population. This lymphocytic response may represent an immune reaction to the xenograft and may be due specifically to remnant cellular elements [17, 40] or antibiotic [41, 42] that likely remain in the fascia even after processing [17, 40]. Host recognition of the slight molecular differences in the proteoglycans and glycoproteins in xenogenic tissue [43, 44] or changes to protein structure after processing [45] may have also triggered the adaptive immune system. Thus, fascia ECM would likely elicit less chronic inflammation than seen here, if used as an allograft in human patients.

TS-HA treated fascia, with or without cross-linking, exhibited a heightened macrophage response compared to water controls. The extent to which the mechanism leading to this outcome is the same for both groups is unknown, but may involve at least some common elements. Because TS-HA treatment tended to increase the cross-sectional area of fascia

grafts in both groups and the added TS-HA was distributed around the fascicle bundles, we conclude that the inter-fascicular space likely expanded to accommodate the added TS-HA. In the case of treated fascia without cross-linking, TS-HA is presumably leached from these spaces within hours to days after implantation (as supported by our in vitro results), allowing for increased cellular infiltration. Further, given that the in vivo half-life of HA is on the order of hours [46], the macrophage response in the uncross-linked group may be in part a downstream consequence of a bolus release of HA during the early phases of healing. In the case of treated fascia with cross-linking, the heightened macrophage response may be a consequence of continued phagocytic activity against the persistent TS-HA hydrogel. Furthermore, CD44-mediated binding of monocytes/macrophages to HA is enhanced upon a covalent association with heavy chains derived from inter-α-inhibitor, a protease inhibitor found in serum [47, 48]. Binding of monocytes/macrophages to HA has been demonstrated in both in vitro and in vivo models of inflammation and could explain the heightened macrophage response observed in this study. Regardless of the mechanism, it is important to note that the heightened macrophage response was not associated with a change in macrophage polarization. TS-HA treated fascia with or without cross-linking was predominantly infiltrated by M2 pro-remodeling macrophages, suggestive of constructive remodeling by tissue repair and regeneration [19, 20].

The observation of giant cells was unique to cross-linked treated fascia, suggesting that regions of the TS-HA hydrogel could not be phagocytosed by macrophages, thereby prompting giant cell formation to breakdown the aggregates by degradative agents. Although graft degradation is expected in the course of host incorporation and tissue remodeling, premature or extensive breakdown of the matrix before host replacement with functional tissue can result in a detrimental loss of mechanical properties [49]. The extent to which the giant cell response affects the mechanical properties of TS-HA treated fascia is the subject of our ongoing work. Although TS-HA treated fascia with cross-linking was characterized by multinucleated giant cells—the hallmark of the foreign body response—no fibrous capsule was observed at 3 months. We would not expect fibrous encapsulation of TS-HA treated fascia with cross-linking to occur at later time points, since encapsulation of other ECM grafts such as Permacol (isocyanate-cross-linked porcine dermis) was apparent as early as seven days after implantation [50].

TS-HA treated fascia without cross-linking trended towards an increase in cellularity compared to water treated fascia. As previously mentioned, the expanded inter-fascicular space that becomes devoid of TS-HA after implantation may allow for greater cellular infiltration. This hypothesis is consistent with our finding that treated fascia with cross-linking did not exhibit the same increased cellularity. In fact, cross-linked TS-HA treated fascia had fewer fibroblast-like cells than water or uncross-linked treated fascia, suggesting that TS-HA hydrogel negatively impacts fibroblast infiltration, adhesion, and/or proliferation. Inhibition of these cell functions may be the result of the impenetrable, smooth nature of a HA hydrogel which is not conducive to fibroblast attachment [51]. Further elucidating these mechanisms will aid in the development of TS-HA treated fascia as a scaffold supportive of matrix-producing fibroblasts.

While numerous studies have demonstrated that exogenous, high molecular weight HA can inhibit the infiltration, proliferation, and cytokine production of macrophages [28–31, 52, 53], there is an equally large body of evidence showing that HA can be associated with macrophage activation and adhesion as well as foreign body giant cell response [54–58]. It is important to note that previous studies investigated HA in endogenous, soluble, injectable, or pure hydrogel form, in either cell culture or in vivo injury models; all of which differ from the form of HA and in vivo model system employed in this study. To the best of our knowledge, there is no precedent for the investigation of in vivo host response to an ECM

impregnated with a HA hydrogel, limiting comparison of our results to previous work. However, in one recent study, Brown et al. showed that bladder ECM treated with disulfide cross-linked, thiol-modified HA facilitated and expedited the infiltration of bladder smooth muscle cells into bladder ECM in cell culture [59]. Since disulfide cross-linking is reversible and the incorporated HA could be leached or degraded over time (unlike dityramine cross-linking), this result is consistent with our observation of heightened cellularity in TS-HA treated fascia without cross-linking.

Since fascia grafts were not radioactively labeled in our study, the processes of resorption and host tissue deposition could not be distinguished from each other. As a means to estimate the net effect of resorption and deposition over time, post-implantation cross-sectional area at 1 and 3 months was measured. The significant decrease in cross-sectional area from 1 to 3 months may be a consequence of greater matrix resorption than deposition and/or simply the resolution of an initial edema/swelling. Future work should investigate the effect of TS-HA treatment specifically on the remodeling of the fascia matrix over time.

This study is not without limitations. Although treated fascia patches were selected for implantation based on the criterion that their mean TS-HA content fell within the range of 5–10 μg/mg, the variable nature of the histologic scores within a single experimental group could be attributed to the variability in TS-HA content from one graft to another. Our ongoing development of treatment methodologies aims to obtain a more uniform TS-HA concentration within and between treated fascia grafts. Second, the latest implantation time point investigated in this study was 3 months. Certainly, longer implantation times are necessary to ascertain the extent to which the lymphocyte aggregation clears, the giant cell population diminishes, the TS-HA hydrogel is degraded, and to observe end-stage tissue remodeling. However, 3 months is sufficient for predicting either a constructive tissue remodeling outcome or a pro-inflammatory (destructive) tissue remodeling outcome [19]. Lastly, only treated fascia grafts with a mean TS-HA content of 5–10 μg/mg and only one molecular weight (0.9–1 M Da) were investigated. A dose- or molecular-weight-dependent histologic response to TS-HA amount is likely and should be further investigated.

5 Conclusions

This study is novel in that it characterizes the host response to decellularized fascia ECM and TS-HA treated fascia ECM with or without cross-linking. TS-HA treated fascia with cross-linking had similar lymphocyte and plasma cell densities, greater macrophage and giant cell densities, and a lower density of fibroblast-like cells than water treated controls. Treated fascia with or without cross-linking exhibited a predominantly M2, pro-remodeling macrophage profile similar to water controls, which is suggestive of constructive tissue remodeling. Our findings suggest that augmentation of an ECM, in particular human fascia lata, with HA can alter the host response to the ECM. This work provides guidance for the ongoing development of HA treated extracellular matrices as scaffolds for augmenting the repair of soft tissues. Future work will investigate alternative treatment methods and the dose- and molecular-weight-dependent host response to HA treated fascia ECM.

Acknowledgments

This study was financially supported by the National Institutes of Health (NIAMS Grant # R01AR056633, F31AR057305, T32AR50959) and the Ohio Third Frontier (Grant # BRTT05-30). The authors would like to acknowledge the Musculoskeletal Transplant Foundation for their fascia donation, Lifecore Biomedical for their TS-HA donation, and Michael Braun (Biomedical Engineering Histology Core, Cleveland Clinic) for the histologic preparation of the H&E stained sections.

References

1. Badylak SF, Lantz GC, Coffey A, Geddes LA. Small intestinal submucosa as a large diameter vascular graft in the dog. J Surg Res. 1989; 47(1):74–80. [PubMed: 2739401]
2. Pavcnik D, Uchida BT, Timmermans HA, Corless CL, O'Hara M, Toyota N, et al. Percutaneous bioprosthetic venous valve: a long-term study in sheep. J Vasc Surg. 2002; 35(3):598–602. [PubMed: 11877716]
3. Badylak S, Obermiller J, Geddes L, Matheny R. Extracellular matrix for myocardial repair. Heart Surg Forum. 2003; 6(2):E20–6. [PubMed: 12716647]
4. Badylak S, Kokini K, Tullius B, Simmons-Byrd A, Morff R. Morphologic study of small intestinal submucosa as a body wall repair device. J Surg Res. 2002; 103(2):190–202. [PubMed: 11922734]
5. Buinewicz B, Rosen B. Acellular cadaveric dermis (AlloDerm): a new alternative for abdominal hernia repair. Ann Plast Surg. 2004; 52(2):188–94. [PubMed: 14745271]
6. Piechota HJ, Gleason CA, Dahms SE, Dahiya R, Nunes LS, Lue TF, et al. Bladder acellular matrix graft: in vivo functional properties of the regenerated rat bladder. Urol Res. 1999; 27(3):206–13. [PubMed: 10422823]
7. Jones JS, Rackley RR, Berglund R, Abdelmalak JB, DeOrco G, Vasavada SP. Porcine small intestinal submucosa as a percutaneous mid-urethral sling: 2-year results. BJU Int. 2005; 96(1):103–6. [PubMed: 15963130]
8. Yim H, Cho YS, Seo CH, Lee BC, Ko JH, Kim D, et al. The use of AlloDerm on major burn patients: AlloDerm prevents post-burn joint contracture. Burns. 2010; 36(3):322–8. [PubMed: 20080353]
9. Mostow EN, Haraway GD, Dalsing M, Hodde JP, King D. Effectiveness of an extracellular matrix graft (OASIS Wound Matrix) in the treatment of chronic leg ulcers: a randomized clinical trial. J Vasc Surg. 2005; 41(5):837–43. [PubMed: 15886669]
10. Adams JE, Zobitz ME, Reach JS Jr, An KN, Steinmann SP. Rotator cuff repair using an acellular dermal matrix graft: an in vivo study in a canine model. Arthroscopy. 2006; 22(7):700–9. [PubMed: 16843804]
11. Derwin KA, Badylak SF, Steinmann SP, Iannotti JP. Extracellular matrix scaffold devices for rotator cuff repair. J Should Elbow Surg. 2010; 19(3):467–76.
12. Hodde J. Extracellular matrix as a bioactive material for soft tissue reconstruction. ANZ J Surg. 2006; 76(12):1096–100. [PubMed: 17199697]
13. Badylak SF. The extracellular matrix as a scaffold for tissue reconstruction. Semin Cell Dev Biol. 2002; 13(5):377–83. [PubMed: 12324220]
14. Lanza, R.; Langer, R.; Vacanti, JP. Principles of tissue engineering. 3. Maryland Heights: Academic Press; 2007.
15. Badylak SF. Xenogeneic extracellular matrix as a scaffold for tissue reconstruction. Transpl Immunol. 2004; 12(3–4):367–77. [PubMed: 15157928]
16. Whitlock PW, Smith TL, Poehling GG, Shilt JS, Van DM. A naturally derived, cytocompatible, and architecturally optimized scaffold for tendon and ligament regeneration. Biomaterials. 2007; 28(29):4321–9. [PubMed: 17610948]
17. Derwin KA, Baker AR, Spragg RK, Leigh DR, Farhat W, Iannotti JP. Regional variability, processing methods, and biophysical properties of human fascia lata extracellular matrix. J Biomed Mater Res A. 2008; 84(2):500–7. [PubMed: 17618495]
18. Aurora A, McCarron J, Iannotti JP, Derwin K. Commercially available extracellular matrix materials for rotator cuff repairs: state of the art and future trends. J Should Elbow Surg. 2007; 16(5 Suppl):S171–8.
19. Brown BN, Valentin JE, Stewart-Akers AM, McCabe GP, Badylak SF. Macrophage phenotype and remodeling outcomes in response to biologic scaffolds with and without a cellular component. Biomaterials. 2009; 30(8):1482–91. [PubMed: 19121538]
20. Badylak SF, Valentin JE, Ravindra AK, McCabe GP, Stewart-Akers AM. Macrophage phenotype as a determinant of biologic scaffold remodeling. Tissue Eng A. 2008; 14(11):1835–42.
21. Mantovani A, Sica A, Locati M. Macrophage polarization comes of age. Immunity. 2005; 23(4): 344–6. [PubMed: 16226499]

22. Mills CD, Kincaid K, Alt JM, Heilman MJ, Hill AM. M-1/M-2 macrophages and the Th1/Th2 paradigm. J Immunol. 2000; 164(12):6166–73. [PubMed: 10843666]
23. Stout RD, Jiang C, Matta B, Tietzel I, Watkins SK, Suttles J. Macrophages sequentially change their functional phenotype in response to changes in microenvironmental influences. J Immunol. 2005; 175(1):342–9. [PubMed: 15972667]
24. Mantovani A, Sica A, Sozzani S, Allavena P, Vecchi A, Locati M. The chemokine system in diverse forms of macrophage activation and polarization. Trends Immunol. 2004; 25(12):677–86. [PubMed: 15530839]
25. Toole BP, Gross J. The extracellular matrix of the regenerating newt limb: synthesis and removal of hyaluronate prior to differentiation. Dev Biol. 1971; 25(1):57–77. [PubMed: 5557969]
26. Cantor JO, Nadkarni PP. Hyaluronan: the Jekyll and Hyde molecule. Inflamm Allergy Drug Targets. 2006; 5(4):257–60. [PubMed: 17168797]
27. Noble PW. Hyaluronan and its catabolic products in tissue injury and repair. Matrix Biol. 2002; 21(1):25–9. [PubMed: 11827789]
28. Schimizzi AL, Massie JB, Murphy M, Perry A, Kim CW, Garfin SR, et al. High-molecular-weight hyaluronan inhibits macrophage proliferation and cytokine release in the early wound of a preclinical postlaminectomy rat model. Spine J. 2006; 6(5):550–6. [PubMed: 16934726]
29. Nakamura K, Yokohama S, Yoneda M, Okamoto S, Tamaki Y, Ito T, et al. High, but not low, molecular weight hyaluronan prevents T-cell-mediated liver injury by reducing proinflammatory cytokines in mice. J Gastroenterol. 2004; 39(4):346–54. [PubMed: 15168246]
30. Sheehan KM, DeLott LB, West RA, Bonnema JD, DeHeer DH. Hyaluronic acid of high molecular weight inhibits proliferation and induces cell death in U937 macrophage cells. Life Sci. 2004; 75(26):3087–102. [PubMed: 15488890]
31. Yasuda T. Hyaluronan inhibits prostaglandin E2 production via CD44 in U937 human macrophages. Tohoku J Exp Med. 2010; 220(3):229–35. [PubMed: 20208419]
32. Docherty R, Forrester JV, Lackie JM, Gregory DW. Glycos-aminoglycans facilitate the movement of fibroblasts through three-dimensional collagen matrices. J Cell Sci. 1989; 92(Pt 2):263–70. [PubMed: 2506200]
33. Yagi M, Sato N, Mitsui Y, Gotoh M, Hamada T, Nagata K. Hyaluronan modulates proliferation and migration of rabbit fibroblasts derived from flexor tendon epitenon and endotenon. J Hand Surg Am. 2010; 35(5):791–6. [PubMed: 20438995]
34. Campo GM, Avenoso A, Campo S, D'Ascola A, Nastasi G, Calatroni A. Molecular size hyaluronan differently modulates toll-like receptor-4 in LPS-induced inflammation in mouse chondrocytes. Biochimie. 2010; 92(2):204–15. [PubMed: 19879319]
35. Campo GM, Avenoso A, Campo S, D'Ascola A, Traina P, Rugolo CA, et al. Differential effect of molecular mass hyaluronan on lipopolysaccharide-induced damage in chondrocytes. Innate Immun. 2010; 16(1):48–63. [PubMed: 19710088]
36. Lyle DB, Breger JC, Baeva LF, Shallcross JC, Durfor CN, Wang NS, et al. Low molecular weight hyaluronic acid effects on murine macrophage nitric oxide production. J Biomed Mater Res A. 2010; 94(3):893–904. [PubMed: 20336750]
37. Darr A, Calabro A. Synthesis and characterization of tyramine-based hyaluronan hydrogels. J Mater Sci Mater Med. 2009; 20(1):33–44. [PubMed: 18668211]
38. Calabro A, Benavides M, Tammi M, Hascall VC, Midura RJ. Microanalysis of enzyme digests of hyaluronan and chondroitin/dermatan sulfate by fluorophore-assisted carbohydrate electrophoresis (FACE). Glycobiology. 2000; 10(3):273–81. [PubMed: 10704526]
39. Lin W, Shuster S, Maibach HI, Stern R. Patterns of hyaluronan staining are modified by fixation techniques. J Histochem Cytochem. 1997; 45(8):1157–63. [PubMed: 9267476]
40. Zheng MH, Chen J, Kirilak Y, Willers C, Xu J, Wood D. Porcine small intestine submucosa (SIS) is not an acellular collagenous matrix and contains porcine DNA: possible implications in human implantation. J Biomed Mater Res B. 2005; 73(1):61–7.
41. Shirley SF, Little JR. Immunopotentiating effects of amphotericin B. II. Enhanced in vitro proliferative responses of murine lymphocytes. J Immunol. 1979; 123(6):2883–9. [PubMed: 501095]

42. Vonk AG, Netea MG, Denecker NE, Verschueren IC, van der Meer JW, Kullberg BJ. Modulation of the pro- and anti-inflammatory cytokine balance by amphotericin B. J Antimicrob Che-mother. 1998; 42(4):469–74.
43. Fox A, Harrison LC. Innate immunity and graft rejection. Immunol Rev. 2000; 173:141–7. [PubMed: 10719675]
44. Tauro JC, Parsons JR, Ricci J, Alexander H. Comparison of bovine collagen xenografts to autografts in the rabbit. Clin Ort-hop Relat Res. 1991; 266:271–84.
45. Badylak SF, Gilbert TW. Immune response to biologic scaffold materials. Semin Immunol. 2008; 20(2):109–16. [PubMed: 18083531]
46. Lindholm A, Roneus B, Lindblad G, Jones B. Hyaluronan turnover in the synovial fluid in metacarpophalangeal–and middle carpal joints in standardbred horses. Acta Vet Scand. 1996; 37(2):147–51. [PubMed: 8767693]
47. Lauer ME, Fulop C, Mukhopadhyay D, Comhair S, Erzurum SC, Hascall VC. Airway smooth muscle cells synthesize hyaluronan cable structures independent of inter-alpha-inhibitor heavy chain attachment. J Biol Chem. 2009; 284(8):5313–23. [PubMed: 19075022]
48. Zhuo L, Kanamori A, Kannagi R, Itano N, Wu J, Hamaguchi M, et al. SHAP potentiates the CD44-mediated leukocyte adhesion to the hyaluronan substratum. J Biol Chem. 2006; 281(29): 20303–14. [PubMed: 16702221]
49. Badylak SF, Freytes DO, Gilbert TW. Extracellular matrix as a biological scaffold material: structure and function. Acta Bio-mater. 2009; 5(1):1–13.
50. Valentin JE, Badylak JS, McCabe GP, Badylak SF. Extracellular matrix bioscaffolds for orthopaedic applications. A comparative histologic study. J Bone Joint Surg Am. 2006; 88(12): 2673–86. [PubMed: 17142418]
51. Shu XZ, Ghosh K, Liu Y, Palumbo FS, Luo Y, Clark RA, et al. Attachment and spreading of fibroblasts on an RGD peptide-modified injectable hyaluronan hydrogel. J Biomed Mater Res A. 2004; 68(2):365–75. [PubMed: 14704979]
52. Proctor M, Proctor K, Shu XZ, McGill LD, Prestwich GD, Orlandi RR. Composition of hyaluronan affects wound healing in the rabbit maxillary sinus. Am J Rhinol. 2006; 20(2):206–11. [PubMed: 16686391]
53. Yasuda T. Hyaluronan inhibits cytokine production by lipopolysaccharide-stimulated U937 macrophages through down-regulation of NF-kappaB via ICAM-1. Inflamm Res. 2007; 56(6): 246–53. [PubMed: 17607549]
54. Wallet MA, Wallet SM, Guiulfo G, Sleasman JW, Goodenow MM. IFNgamma primes macrophages for inflammatory activation by high molecular weight hyaluronan. Cell Immunol. 2010; 262(2):84–8. [PubMed: 20299009]
55. Savani RC, Hou G, Liu P, Wang C, Simons E, Grimm PC, et al. A role for hyaluronan in macrophage accumulation and collagen deposition after bleomycin-induced lung injury. Am J Respir Cell Mol Biol. 2000; 23(4):475–84. [PubMed: 11017912]
56. Jokela TA, Lindgren A, Rilla K, Maytin E, Hascall VC, Tammi RH, et al. Induction of hyaluronan cables and monocyte adherence in epidermal keratinocytes. Connect Tissue Res. 2008; 49(3):115–9. [PubMed: 18661324]
57. Lemperle G, Morhenn V, Charrier U. Human histology and persistence of various injectable filler substances for soft tissue augmentation. Aesthetic Plast Surg. 2003; 27(5):354–66. [PubMed: 14648064]
58. Al-Shraim M, Jaragh M, Geddie W. Granulomatous reaction to injectable hyaluronic acid (Restylane) diagnosed by fine needle biopsy. J Clin Pathol. 2007; 60(9):1060–1. [PubMed: 17761744]
59. Brown AL, Srokowski EM, Shu XZ, Prestwich GD, Woodhouse KA. Development of a model bladder extracellular matrix combining disulfide cross-linked hyaluronan with decellularized bladder tissue. Macromol Biosci. 2006; 6(8):648–57. [PubMed: 16881043]

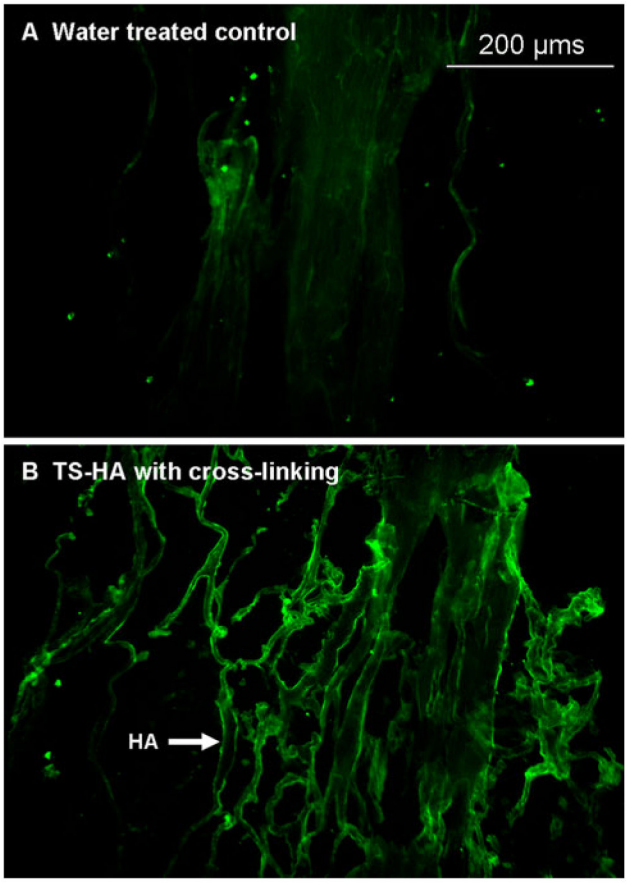

Fig. 1.
Representative images of bHABP stained fascia grafts: **a** water treated control and **b** TS-HA treated with cross-linking (×100). The incorporated TS-HA was distributed throughout the fascia matrix, primarily around large fascicle bundles

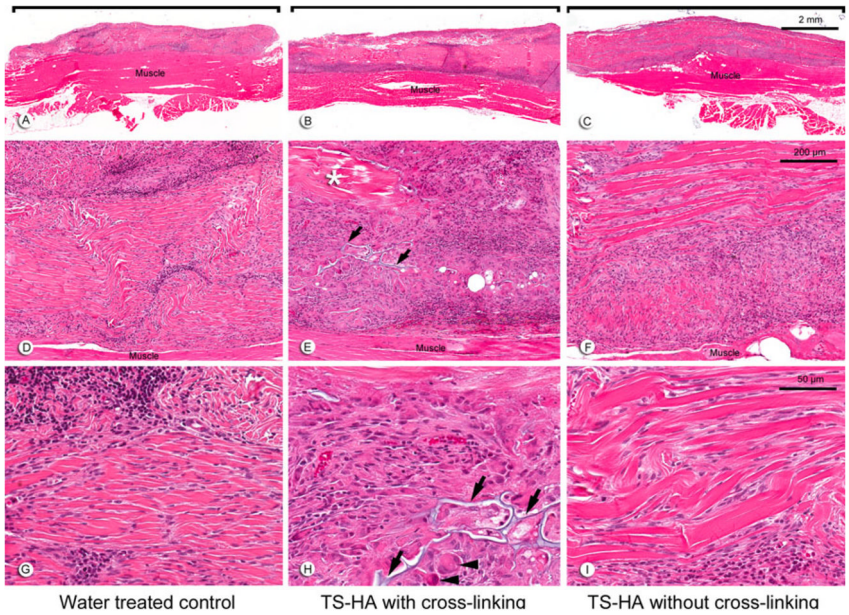

Fig. 2.

Representative H&E images at 1 month of: **a**, **d**, **g** water treated control; **b**, **e**, **h** TS-HA with cross-linking; and **c**, **f**, **i** TS-HA without cross-linking. **a**–**c** (×10) Fascia grafts (*brackets*) were still visible and discernable from the underlying abdominal skeletal muscle. **d**–**f** (×100) Remnant fascia architecture was identifiable as longitudinal, collagenous bands. Grafts exhibited a variable distribution of cellular infiltrates and acellular, collagenous regions (*asterisk*), as demonstrated in treated fascia with cross-linking (**e**). **g**–**i** (×400) Grafts were heavily infiltrated by chronic inflammatory cells, which were predominantly lymphocytes, as demonstrated in water controls (**g**). In cross-linked treated fascia, TS-HA hydrogel was discernable (*arrows*) and surrounded by multinucleated giant cells (**h**, *arrowheads*). Spindle-shaped, fibroblast-like cells heavily infiltrated the grafts, often between the collagenous bands, as demonstrated in uncross-linked treated fascia (**i**)

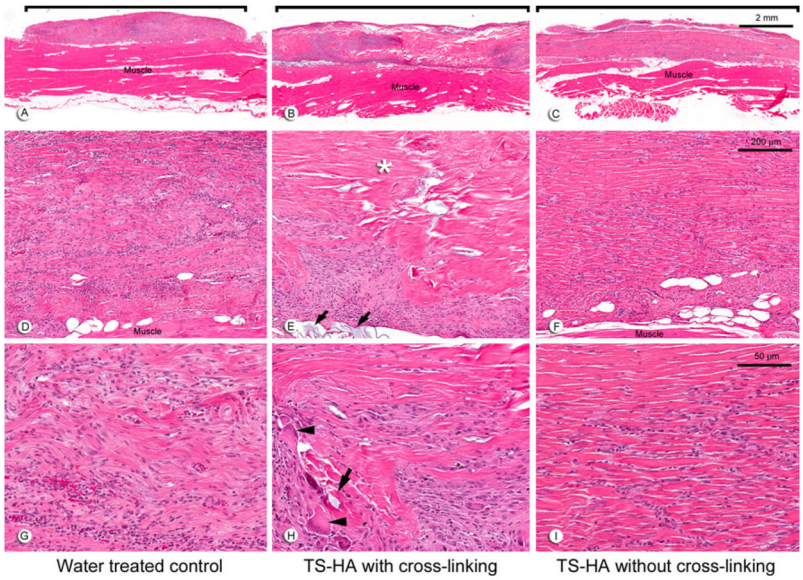

Fig. 3.

Representative H&E images at 3 months of: **a**, **d**, **g** water treated control; **b**, **e**, **h** TS-HA with cross-linking; and **c**, **f**, **i** TS-HA without cross-linking. **a**–**c** (×10) Fascia grafts (*brackets*) were still visible and discernable from the underlying abdominal skeletal muscle. **d**–**f** (×100) A chronic inflammatory response was observed in all grafts at 3 months, but to a lesser extent than at 1 month for water control and uncross-linked treated fascia. Cross-linked treated grafts exhibited a variable distribution of cellular infiltrates, acellular regions (*asterisk*), and TS-HA hydrogel (**e**, *arrows*). **g**–**i** (×400) Fibroblast-like cells and disorganized connective tissue were observed in all groups, as demonstrated in water control grafts (**g**). In TS-HA with cross-linking grafts, hydrogel (*arrows*) and giant cells (*arrowheads*) were observed (**h**). Spindle-shaped, fibroblast-like cells heavily infiltrated the grafts, often between collagenous bands, as demonstrated in uncross-linked treated fascia (**i**)

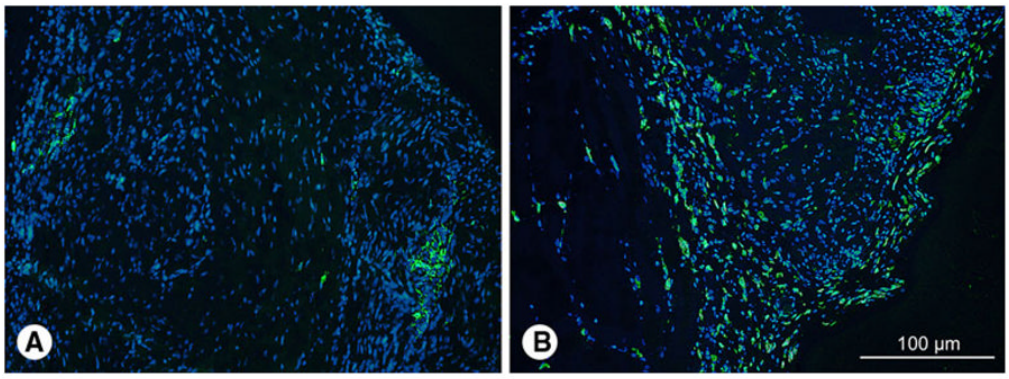

Fig. 4.

Representative immunostaining of: **a** CCR7 and **b** CD163 immunostaining at 3 months of water treated control (×200). CCR7+ M1 macrophages were often focally concentrated in small clusters, and CD163+ M2 macrophages were localized at the periphery of the grafts. CCR7 and CD163 staining was similar for TS-HA treated fascia, with or without cross-linking. Nuclei were stained with DAPI

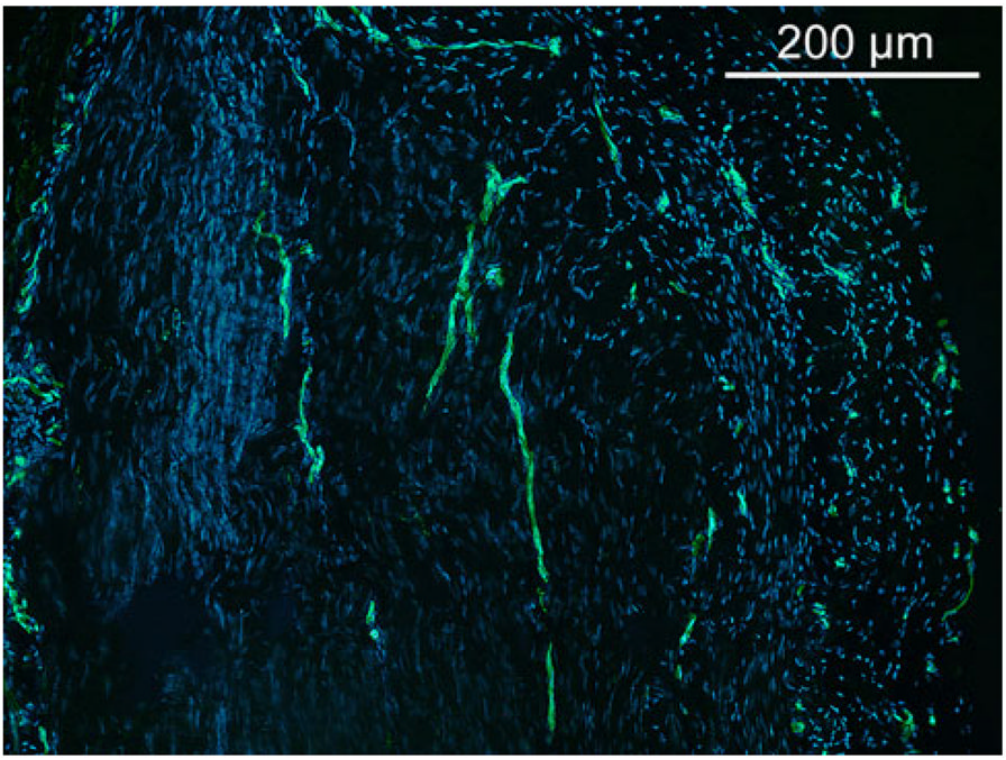

Fig. 5.

Representative CD31 immunostaining for vascularization at 3 months of water treated control (×100). Capillary vessels are lined with CD31+ endothelial cells. A few longitudinally oriented capillaries are shown in the central area of the graft. Capillary density was higher at the periphery of the graft. CD31 staining was similar for TS-HA treated fascia, with or without cross-linking. Nuclei were stained with DAPI

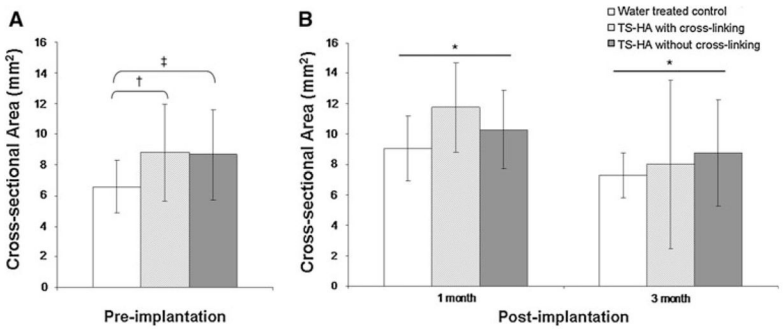

Fig. 6.

a Pre-implantation and **b** post-implantation cross-sectional area of water treated control, TS-HA with cross-linking, and TS-HA without cross-linking treated fascia. †, ‡TS-HA treated fascia pieces, with ($P = 0.06$) or without cross-linking ($P = 0.08$), trended towards greater pre-implantation cross-sectional area than water controls. *Post-implantation cross-sectional area significantly decreased from 1 to 3 months for all groups ($P = 0.02$). There was no significant difference in cross-sectional area among groups at either post-implantation time point

Table 1

Histologic scoring system adapted from ISO 10993-6 standard

Cell type/response	Score				
	0	**1**	**2**	**3**	**4**
Inflammatory cell outcomes					
Lymphocytes	0	Rare—1–5/hpf	5–10/hpf	Heavy infiltrate	Packed
Plasma cells	0	Rare—1–5/hpf	5–10/hpf	Heavy infiltrate	Packed
Macrophages	0	Rare—1–5/hpf	5–10/hpf	Heavy infiltrate	Packed
Giant cells	0	Rare—1–2/hpf	3–5/hpf	Heavy infiltrate	Packed
$CCR7^+$ pro-inflammatory M1 macrophages	0	Rare—1–5/hpf	5–10/hpf	Heavy infiltrate	Packed
$CD163^+$ pro-remodeling M2 macrophages	0	Rare—1–5/hpf	5–10/hpf	Heavy infiltrate	Packed
Non-inflammatory outcomes					
Total cellularity	–	< 25%	26–50%	51–75%	> 75%
Fibroblasts	0	Rare—100/hpf	100–1000/hpf	Heavy infiltrate	Packed
$CD31^+$ epithelial cells (neovascularization)	0	Minimal capillary proliferation, focal, 1–3 buds	Groups of 4–7 capillaries with supporting fibroblastic structures	Broad band of capillaries with supporting structures	Extensive band of capillaries with supporting fibroblastic structures

hpf high powered field (×400)

Table 2

HA content (mean ± SD) of treated 5 × 5 cm fascia grafts at time zero and after the in vitro retention (IVR) experiment

Treatment group	Time zero (μg/mg$_{DW}$)	IVR (μg/mg$_{DW}$)
Water treated control	0.2 ± 0.1	–
TS-HA with cross-linking	7.6 ± 2.3	8.7 ± 2.0‡
TS-HA without cross-linking	7.8 ± 1.8†	2.7 ± 1.5†,‡

n = 8 grafts per group (triplicate data not shown)

†,‡Like symbols indicate significant difference (P < 0.001)

Table 3

Mean (range) histologic scores for inflammatory cell outcomes

Time point	Experimental group	Inflammatory cell outcomes					
		Lymphocytes	Plasma cells	Macrophages	Giant cells	CCR7$^+$ pro-inflammatory M1 macrophages	CD163$^+$ pro-remodeling M2 macrophages
1 month	Water treated control	3 (3–3)	2 (1–3)	2.3^{a,b} (1–3)	0.8^a (0–1)	1 (1–1)	2.5 (2–3)
	TS-HA with cross-linking	2.5 (1–3)	2.1 (1–4)	3.1^a (2–4)	2.8^{a,b} (1–4)	1 (1–1)	2.8 (2–3)
	TS-HA without cross-linking	3 (2–4)	1.5 (1–3)	2.8^b (1–4)	1.4^b (0–3)	1 (1–1)	2.8 (2–3)
3 month	Water treated control	2.9 (2–3)	0.9 (0–2)	1.5^{c,d} (1–3)	0.8^c (0–3)	1 (1–1)	2.3 (2–3)
	TS-HA with cross-linking	2.6 (2–3)	1.8 (0–4)	2.8^c (1–4)	2.8^{c,d} (0–4)	1 (1–1)	2.3 (2–3)
	TS-HA without cross-linking	2.6 (2–3)	1.1 (0–2)	2.4^d (2–3)	0.6^d (0–1)	0.8 (0–1)	2.0 (2–2)

Like letters indicate significant differences for an outcome across experimental groups within each time point ($P \leq 0.001$)

Across all groups, plasma cell ($P = 0.02$), macrophage ($P = 0.03$), and CD163$^+$ macrophage ($P = 0.02$) scores decreased with time

In all groups at both time points, the density of CD163$^+$ M2 macrophages was greater than CCR7$^+$ M1 macrophages ($P < 0.0001$)

$n = 8$ per group per time point

Table 4

Mean (range) histologic scores for non-inflammatory outcomes

Time point	Experimental group	Non-inflammatory outcomes		
		Total cellularity	Fibroblasts	$CD31^+$ epithelial cells (neovascularization)
1 month	Water treated control	2.1† (1–3)	2.9[a] (1–4)	2.3 (2–3)
	TS-HA with cross-linking	2.1 (1–3)	1.4[a,b] (0–3)	1.8 (1–2)
	TS-HA without cross-linking	2.5† (1–4)	2.9[b] (1–4)	2.5 (2–3)
3 month	Water treated control	2† (1–3)	2.5[c] (2–4)	2.0 (2–2)
	TS-HA with cross-linking	2.5 (1–4)	1.4[c,d] (0–3)	1.8 (1–2)
	TS-HA without cross-linking	3.1† (2–4)	3.3[d] (2–4)	1.8 (1–2)

Like letters indicate significant differences for an outcome across experimental groups within each time point ($P \leq 0.0001$)

$CD31^+$ epithelial cells (neovascularization) scores trended toward a decrease with time ($P = 0.10$)

$n = 8$ per group per time point

† Indicates a trend ($P = 0.09$)